MODE II FRACTURE BEHAVIOR OF BONDED VISCOELASTIC THERMAL COMPRESSED WOOD

*Andreja Kutnar**
Graduate Student
Department of Wood Science and Technology
Biotechnical Faculty
University of Ljubljana
1000 Ljubljana, Slovenia

Frederick A. Kamke†
Professor

John A. Nairn†
Professor
Department of Wood Science and Engineering
Oregon State University
Corvallis, OR 97331-5751

Milan Sernek†
Associate Professor
Department of Wood Science and Technology
Biotechnical Faculty
University of Ljubljana
1000 Ljubljana, Slovenia

(Received November 2007)

Abstract. The influence of viscoelastic thermal compression (VTC) of wood on bonding performance was studied. Mode-II (shear mode) fracture of the bonded interphase was performed using the over-notched and end-notched flexure methods. The study examined four groups of specimens; a control and VTC specimens with three different degrees of densification (63, 98, and 132%). The specimens were bonded with phenol-formaldehyde (PF) adhesive. Prior to fracture testing, the bonded interphase was examined and the effective penetration (EP) of PF into the capillary structure of wood was measured. The results showed that EP was greatest in the control wood specimens, but in the case of the VTC specimens decreased with increasing degree of densification. The mode-II fracture performance of the VTC wood specimens with PF differed from the control wood specimens. In the control specimens, the mode-II crack propagation occurred in the interphase, while in the VTC specimens the crack diverted away from the interphase into the VTC wood. A hypothesis of relative shear resistance was used to explain the bonding performance of the control and VTC specimens.

Keywords: Densification, VTC, bond line, mode-II fracture toughness, over-notched flexure, end-notched flexure.

INTRODUCTION

The densification process, termed viscoelastic thermal compression (VTC), increases the density of wood by means of mechanical compression perpendicular to the longitudinal direction. The VTC process softens the wood above the glass transition temperature, using heat and steam prior to compression. The moisture content of the wood is transient during the compression, thus inducing a mechano-sorption effect

* Corresponding author: andreja.kutnar@siol.net
† SWST member

and further softening the wood (Kamke 2004; Kamke and Sizemore 2005). Because of hydro, thermal, and mechanical treatments in the VTC process, the morphology and chemical composition of the wood surface are changed. Therefore, adhesion (ie mechanical interlocking, physical forces of attraction, and covalent chemical bonds) between wood surface and adhesive is expected to be altered depending on the parameters of the VTC densification process.

Increased density, and consequently decreased porosity, of the VTC wood affects adhesive flow and penetration. The void volume of the VTC wood can be drastically decreased depending on the degree of densification. The depth and direction that an adhesive flows in the VTC wood will therefore be much different than in normal wood. Exposure of wood to high temperatures during VTC processing can reduce the surface wettability of the VTC wood. Wettability of wood that is exposed to high temperature or heat treated is decreased (Sernek et al 2004; Petrissans et al 2003; Follrich et al 2006; Jennings et al 2006; Gérardin et al 2007). The heat-treated wood becomes hydrophobic, less polar, and rather repellent to water, which may impede adequate wetting of the surface with waterborne adhesives.

Almost any material can be bonded using current technology. Research shows that densified wood can be bonded using a polymeric diphenylmethane diisocyanate adhesive and phenol-formaldehyde (PF) film adhesive, as was demonstrated by mode-I fracture testing (Jennings et al 2005). However, information on bonding performance of densified wood using other adhesive systems is lacking. Therefore, the aim of our research was to investigate PF bond performance of VTC wood through use of fracture toughness testing.

Fracture mechanics concepts are effectively used to simulate the actual fracture response of adhesively bonded structures. Interlaminar fracture toughness can be measured in various fracture modes. The most commonly used is mode-I fracture testing (Schmidt 1998; Gagliano and Frazier 2001; Sernek et al 2004; Jennings et al 2005), where a double-cantilever beam (DCB) specimen is loaded in tension perpendicular to the bonded interface. However, it was shown that in adhesively bonded joints, mode II, in-plane shear mode fracture, is also a major contributor to crack propagation (Wang and Qiao 2003). The initiation of cracks in mode-II fracture is produced by relative horizontal displacement of the bonded surfaces of the specimen. The subsequent rotation and opening of these cracks (which produce the fracture surfaces) are not considered in the data analysis (Davies et al 1998).

The following six test configurations are available for measuring mode-II fracture toughness: end-notched flexure (ENF), stabilized ENF (SENF), end-loaded split (ELS), four-point bending ENF (4ENF), over-notched flexure (ONF), and tapered ENF (TENF) coupons (Szekrenyes 2005). All of these specimens have advantages and disadvantages in terms of crack stability and test performance (Szekrenyes and Uj 2005).

The ENF specimen is the most widely used geometry for evaluation of mode-II fracture toughness (Cantwell 1997; Yang and Sun 2000; Yoshihara and Ohta 2000; Szekrenyes and Uj 2005; Kusaka et al 2006). It is essentially a three-point bending beam with a midplane initial crack of a desired length at one end. The ENF specimen is suitable only for determination of the initiation fracture toughness, since the crack growth is unstable. The ONF specimen seems to be the simplest alternative, because stable crack propagation is guaranteed at any crack length (Szekrenyes 2005).

Interlaminar fracture toughness of laminated composites is normally expressed in terms of critical fracture toughness G_c [N/m]. The critical fracture toughness or critical strain energy release rate is the value of the energy required to create two new surfaces at the onset of crack propagation. When fracture toughness G reaches the critical value, ie $G = G_C$, crack initiation or propagation occurs. The fracture toughness can

be calculated in many ways. A common approach is the compliance calibration method, which assumes linear elastic behavior. Using the compliance method, the fracture toughness can be determined as a function of specimen geometry, loading, and crack extension. In this study, the fracture toughness was found by analyzing the structure, and resolving crack-tip normal forces and bending moments (Nairn 2006).

Since VTC wood is expected to be used as a laminated structural material, the design of safe and efficient structures requires a thorough knowledge of adhesive bond performance of VTC wood. In view of the fact that structural material is frequently exposed to bending moments (where fracture often propagates by in-plane shear mode), the objective of this research was to examine interlaminar fracture toughness of the VTC wood specimens bonded with a PF adhesive under mode II. Proper measurement of the mode-II fracture toughness is inherently difficult in laminated wood composites. In the present study, the ONF and ENF specimen geometries were used to test the interlaminar fracture toughness of bonded wood. Penetration of the PF adhesive into the capillary structure of wood was also determined.

MATERIALS AND METHODS

Material Preparation

Low-density hybrid poplar (*Populus deltoides* × *Populus trichocarpa*) from a plantation in northwest Oregon was used in the study. Due to the low density and broad annual rings of hybrid poplar, specimens with mixed radial and tangential orientation were prepared for each degree of densification, and for the control (undensified) specimens. The specimens were 56 mm wide and 170 mm long. The initial thickness of the specimens varied, depending on the intended level of densification to be achieved by the VTC process. Specimens with three different initial thicknesses (4, 5, and 6 mm) were compressed to the same target thickness of 2.5 mm. Thus, three different degrees of densification (63, 98, and 132%) were created (Table 1). The specimens were densified with the VTC process described by Kutnar et al (2008). This multistep process first exposed the wood to 175°C saturated steam and then to dry heat up to 200°C for a total time of 15 min. Aluminium foil was used during the VTC process to protect the surfaces of the specimens from contamination. After the VTC process had been performed, the surfaces of the specimens designed for bonding were protected against exposure to light and air.

TABLE 1. *Characteristics of the VTC and control specimens* (Kutnar et al 2007).

Initial thickness (mm)	Initial density at MC = 0% (kg/m^3)	Density after compression at MC = 0% (kg/m^3)	Degree of densification (%)
4	339	552	63
5	341	676	98
6	340	792	132
6 (control)	331	331	0

Bonding of control and VTC specimens. The specimens were bonded with liquid PF adhesive supplied by Georgia–Pacific Resins, Inc with viscosity 330 mPa · s. This is a commercial product designed for the face layer of oriented strandboard. After conditioning to equilibrium at 20°C and 65% RH, the control samples had a moisture content (MC) of 12%, whereas the VTC specimens had 7% MC.

The fracture tests were conducted in shear parallel to the grain. For majority of the specimens, the grain angle between the bonding surface and the longitudinal fiber axis was small (less than 10°). It has been demonstrated previously that the grain orientation is critical in mode-I fracture testing (Ebewele et al 1979; Jennings et al 2005). However, due to the broad annual rings and small dimensions of the VTC specimens, it was not possible to prepare specimens with precisely controlled grain angles.

Characterization of a Bond Line

A cross-sectional view of the PF adhesive bond line of the control and the VTC wood specimens was made with a fluorescence microscope (Nikon Eclipse E-400) and a color CCD camera

(Roper Scientific Diagnostic Equipment). The effective penetration (EP) of the adhesive into the capillary structure of wood was determined according to Sernek et al (1999). The analyzed surface was located in the middle of the length of the bonded specimens that were bonded in a hot press at 150°C at 700 kPa for 6 min. The adhesive coverage on each bonded surface was 155 g/m^2. An abrasive method was used to prepare the cross-sectional surface of the specimens prior to measurements. This method enabled microscopic examination of the VTC wood bond line in the completely deformed state–in densified, undisturbed form. Furthermore, the method enabled the comparison of the EP in the control and VTC specimens. Namely, common preparation for microscopic examination causes different swelling of the control and VTC specimens from water soaking. Therefore, specimens were soaked in the embedding medium, linseed oil (*Watco Danish Oil, polymerized,* Missouri), under a vacuum, and cured in an oven at 103°C. Embedded specimens were polished with abrasive diamond disks having grit ratings of 600, 1200, and 3000. An abrasive sequence was used to obtain a surface desirable for microscopic analysis. The purpose of the oil was to prevent dust from blocking the lumens.

UV fluorescence permitted digital images to be captured with good color contrast between PF and wood. Manual thresholding by color using an image analysis program (ImageJ 2007) was then used to determine EP of the PF adhesive in the control and in the VTC wood specimens with 16 replicate measurements in each tested group of specimens. The threshold was set for each individual image as the value that would segregate the majority of the adhesive from the wood background. This was a subjective process but consistent for all test specimens. Additionally, the location of the PF adhesive in the cellular structure of the control and VTC wood specimens was determined. The surfaces prepared with the abrasive method could not be used for this examination, because many of the cell lumens were completely collapsed, making identification of cellular structure impossible. Thus, thin sections cut with a sliding microtome from water-soaked specimens were stained with an aqueous solution of 0.5% safranin, and then mounted on glass slides with glycerine. In these slide specimens, there was significant swelling of the wood structure.

Preparation of Fracture Specimens

For the ONF and ENF fracture tests, six-layer beams with the PF adhesive bond line in the center of the beam were formed. Composite beams were fabricated because it is difficult to induce failure by shear when conducting bending tests using specimens with a rectangular cross-section. The reason is that the tensile or compression strength of outer lamina can be reached before the ultimate shear strength of the adhesive bond (Yoshihara and Furushima 2003); therefore deep composite beams were prepared. In narrow and deep beams, the bending performance of the composite test specimens is increased and the shear strength of the adhesive bond in the middle of the specimen is likely to be exceeded. The beam used for the bond performance of the VTC wood is shown in Fig 1. The two central layers were the VTC wood of the same degree of densification, between which the PF adhesive interphase was examined. The VTC wood layers were followed by the control (undensified) wood. The outer layers were again VTC wood of the same degree of densification as the central layers. Thus, these beams were symmetrical, and the sublaminates in arms 1 and 2 of the beam were symmetrical as well. For testing the bond performance of the control wood, the central layers were control wood, whereas the outer layers were made of the VTC wood with a 132% degree of densification. This produced unsymmetrical arms 1 and 2 in specimens for testing the PF adhesive bond performance of the control wood (Fig 2). Hence the calculations of fracture toughness of the control wood were corrected.

A precrack in the ONF and ENF specimens was formed during bonding by inserting a teflon film into the first 55 mm of the interface. The bonded specimens were 15 mm wide, 22 mm thick, and

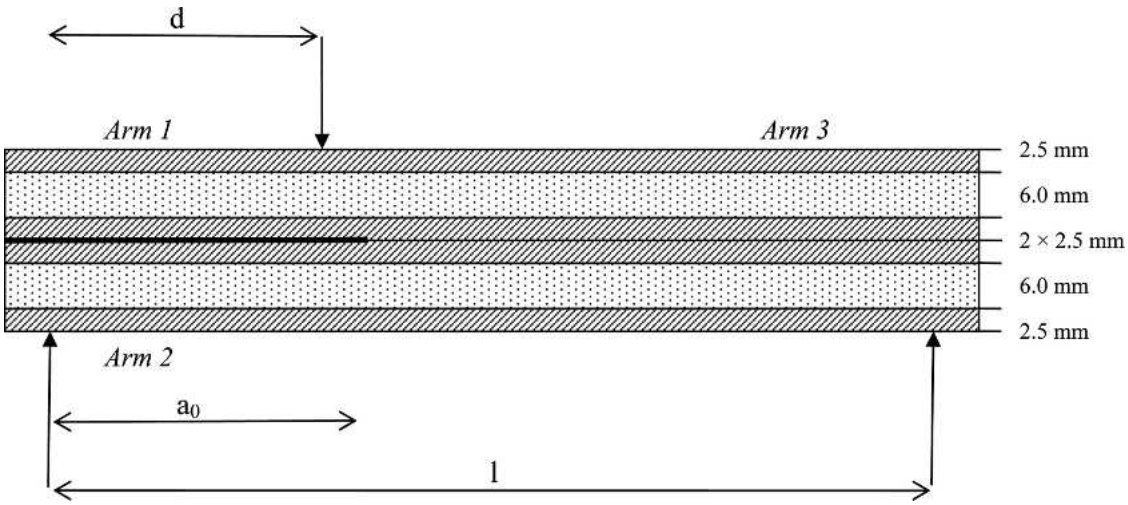

FIGURE 1. Geometrical configuration of the ONF and ENF specimens for testing the PF adhesive bond performance of the VTC wood (diagonal pattern: VTC wood of the same degree of densification; dotted pattern: control). The upper arrow indicates load point.

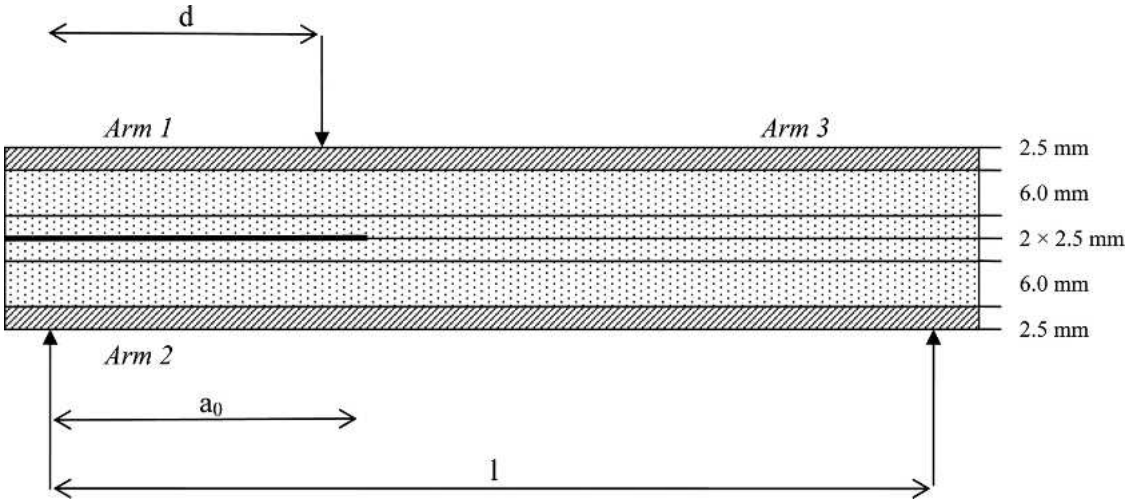

FIGURE 2. Geometrical configuration of the ONF and ENF specimens for testing the PF adhesive bond performance of the control (diagonal pattern: VTC wood with 132% degree of densification; dotted pattern: control). The upper arrow indicates load point.

145 mm long. The composite specimens for the fracture tests (Figs 1 and 2) had adhesive coverage of 155 g/m^2 on each bonded surface and were pressed in a hot press at 150°C and 700 kPa for 30 min. After hot-pressing, the beams were cooled to room temperature and cut into two specimens; for the ONF and ENF tests. Out of the bonded specimens, two 4-mm-wide specimens were cut from the middle, and the lateral edges were discarded. Prior to fracture testing, the specimens were conditioned in a controlled environment room at 65% RH and 20°C until constant weight was obtained.

ONF and ENF experimental procedure. The specimen and loading points for the ONF and

ENF tests are illustrated in Figs 1 and 2. Fracture testing was performed using a standard three-point flexure fixture and a universal testing machine (Sintech 1/G). The specimens were loaded with a crosshead speed of 1 mm/min. The full-span length l was 120 mm for the ONF and ENF tests. The position of the external load d was 40 mm for the ONF test and 60 mm for the ENF (Figs 1 and 2). The specimens were positioned in the fixture to achieve an initial crack length, a_0, of 45 mm. For the ONF test, the interlaminar fracture toughness G_{IIc} was determined in 2-mm increments of the crack length. Due to stability problems, crack propagation in the ENF tests could not be controlled.

During crack propagation in mode II, a matrix of microcracks forms ahead of the crack tip, which eventually coalesces. Therefore, definition of the true crack length was difficult. In this study it was determined using Digital Image Correlation (DIC), which is an optical method to measure deformation on an object's surface. A detailed description of DIC is provided by Hung and Voloshin (2003). Briefly, DIC compares two images acquired at different states –before and after deformation. These images are digitized and stored in a computer for analysis. The method tracks the two-dimensional displacement of identifiable features within a subset of the area of interest. The displacement data are then matched to the loading data. To create a characteristic pattern on the specimen surface, the specimens were coated with white paint followed by a random speckled pattern of black paint.

An example of the measurement of the crack length is presented in Fig 3. For every position of the crack tip, the applied load was known; hence G_{IIc} could be calculated. During mode-II tests, images of the beams under load were captured every 4 s. Acquired images were then analyzed by DIC. Various trial and error methods provided an idea of the best pixel resolution, outer limits of included angle between the cameras, lighting conditions, and adequacy of the speckle pattern. All these parameters are subjective or qualitative in nature and most of them are

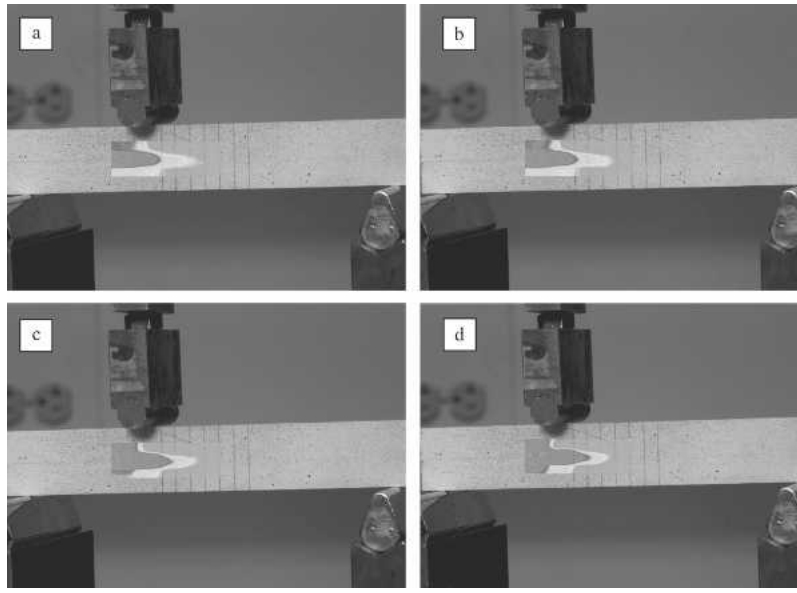

FIGURE 3. Measurement of the crack length by DIC. Two-dimensional strain measurements are superimposed over the test specimen. The ending of dark region surrounded by the white halo represents the crack tip. (a: crack initiation; b: crack length 47 mm; c: crack length 50 mm; d: crack length 52 mm).

interrelated, hence a generalized relationship could not be established.

Calculations of interlaminar fracture toughness G_{IIc}. The fracture toughness was calculated by analyzing the structure, resolving crack-tip normal forces and bending moments, and using the general energy release rate analysis in Nairn (2006). The research done by Nairn (2006) extended the methods for calculating energy release rate in cracked laminates to account for heterogeneous laminates. Because the fracture test specimens of the present study were heterogeneous, containing control and VTC wood, the general method was needed to determine energy release rate. The calculations assumed the adhesive layers were thin and well bonded (prior to fracture). In other words, the beam analysis was for the wood layers and did not explicitly include a finite-thickness adhesive layer. The general expression for G_{II} for the cracked multilayered structures used was:

$$G_{II} = 1/2B \times (C_{k1}M_1^2 + C_{k2}M_2^2 - C_{k3}M_3^2) \quad (1)$$

where M_1, M_2, and M_3 are crack-tip moments in arms 1, 2, and 3 (Fig 1 and 2), respectively, C_{k1}, C_{k2}, and C_{k3} are curvature compliances of each arm, and B is specimen width. For ONF specimens, the moments are given by:

$$M_1 = M_2 = [Pa(l - d)/2l] - [P(a - d)/2] \quad (2)$$

$$M_3 = M_1 + M_2 = [d(-a + l)P]/l \quad (3)$$

where a is the crack length, P is the applied load, l is the span length, and d is the position of the applied load.

The curvature compliances for the arms of the VTC testing specimen were determined by a laminated beam analysis (Nairn 2006):

$$C_{k1} = C_{k2} = 12R\lambda^3/[BE_1t_1^3(1 + 2R\lambda(3 + 6\lambda + 4\lambda^2))] \quad (4)$$

$$C_{k3} = 3R\lambda^3/[2BE_1t_1^3(1 + 3(1 + R)\lambda + (3 + 9R)\lambda^2 + 8R\lambda^3)] \quad (5)$$

where $R = E_1/E_2$, $\lambda = t_1/t_2$, and E_1 and E_2 are the moduli of the examined VTC wood and of the control wood, respectively; t_1 is thickness of the VTC wood; t_2 is thickness of the control wood in the beam.

The E_1 and E_2 values were obtained by static three-point bending tests prior to the preparation of the fracture test specimens. For all the specimens, the test span was 100 mm, the load was applied at the midpoint in 3-point bending, and the loading rate was 3 mm/min.

For the control wood specimens (unsymmetrical arms 1 and 2 in Fig 2), the curvature compliances are:

$$C_{k1}^{(c)} = C_{k2}^{(c)} = 12R\lambda^3(1 + \lambda + R\lambda)/[BE_1t_1^3(1 + 4(1 + R)\lambda + 6(1 + 3R)\lambda^2 + 4(1 + 7R)\lambda^3 + (1 + 14R + R^2\lambda^4))] \quad (6)$$

$$C_{k3}^{(c)} = 3R\lambda^3/[2BE_1t_1^3(1 + 3(1 + R)\lambda + (3 + 9R)\lambda^2 + (1 + 7R)\lambda^3)] \quad (7)$$

The calculations for the ENF specimens (beam loaded in the middle of the span) are similar. The only difference is that the crack-tip moments changed to:

$$M_1 = M_2 = a(1 - d)P/2l \quad (8)$$

$$M_3 = a(1 - d)P/l \quad (9)$$

RESULTS AND DISCUSSION

The PF Adhesive Bond Line

Adhesive penetration can be defined as the spatial distance from the interface of the adjoining substrate (Sernek et al 1999). There are different ways of quantifying the adhesive penetration. The EP is calculated as the total area of the adhesive detected in the interphase region of the bond line divided by the width of the observed bond line. For this study, the width of the bond line was the width of the digital images analyzed by ImageJ (1.6 mm). Statistical analysis (Excel Anova: Single Factor) indicated significant differences between the EP of PF adhesive into the control specimens and the VTC specimens of different degrees of densification (p-value 1.12×10^{-16}). The EP was the greatest in the

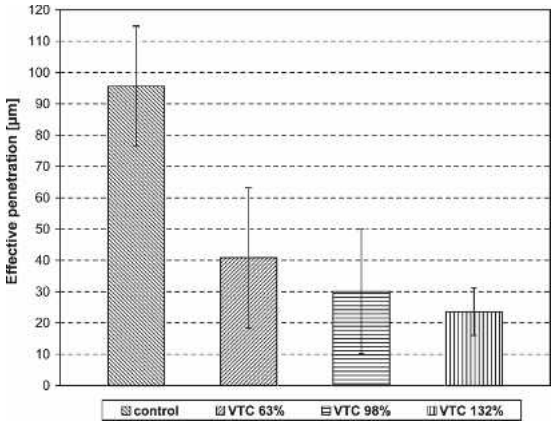

FIGURE 4. The effective penetration of PF adhesive into the control and VTC wood specimens of different degrees of densification.

control wood specimens. In the case of the VTC specimens, EP decreased with the increasing densification (Fig 4). However, the multiple comparison procedure using Fisher's least significant difference (LSD) determined which means were significantly different from others (Table 2). The EP in the VTC specimens with 63% densification was not significantly different from the EP in VTC specimens with 98% densification; and the EP in VTC specimens with 98% densification was not significantly different from the EP in VTC specimens with 132% densification.

Besides this difference in the EP, it was found that the location of the PF adhesive in the cellular structure of control and VTC specimens differed (Fig 5). In the control wood, the adhesive was almost exclusively found in vessel lumens, while in the VTC wood the adhesive was also detected in the fiber and ray lumens. These results are due to the changed porosity of wood as a consequence of densification. Since the vessel lumen volume decreases with increasing degree of densification, the adhesive penetrates into other lumens. The flow of the adhesive follows the direction of least resistance.

It should be also mentioned that because of reduced porosity (and assumed lower permeability) of VTC wood surface, more adhesive squeezed out of the bond line during pressing, in comparison with control wood specimens. This fact is probably reflected in the results of the EP study (Fig 4).

TABLE 2. *Multiple range test with 95% LSD of the EP in the control and VTC wood.*

	Count	Mean [µm]
VTC 132%	16	23.5
VTC 98%	16	30.1
VTC 63%	16	40.8
Control	16	95.6
Contrast	Difference	+/– Limits
Control-VTC 63%	*54.8	12.9
Control-VTC 98%	*65.6	12.9
Control-VTC 132%	*72.1	12.9
VTC 63%-VTC 98%	10.7	12.9
VTC 63%-VTC 132%	*17.3	12.9
VTC 98%-VTC 132%	6.5	12.9

* denotes a statistically significant difference

Modulus of Elasticity

To determine the values of E_1 and E_2 in Eqs 4, 5, 6, and 7, MOE of the control and VTC wood specimens was measured by static three-point bending tests prior to the preparation of the fracture test specimens. Values used in calculations are presented in Table 3. As expected, MOE increased with increasing densification of wood.

Over-notched Flexure

It was found that the ONF geometry was suitable for investigating the crack propagation in the bonded control and the VTC wood specimens, although it was not possible to achieve long crack lengths. This limitation was due to the necessary high loads for continued crack propagation, which caused tensile failure in the outer layer of the beam.

Figure 6 shows the relationship between the crack length a and the mode-II interlaminar fracture toughness G_{IIc} for the ONF specimens. Each curve represents an average value of seven measurements. Because of the small amount of crack propagation that was possible (7 mm), the toughness did not reach a steady-state value. We regarded the curves as the initial portions of toughness resistance curves ("R curves") and compared toughness by shifts of those curves.

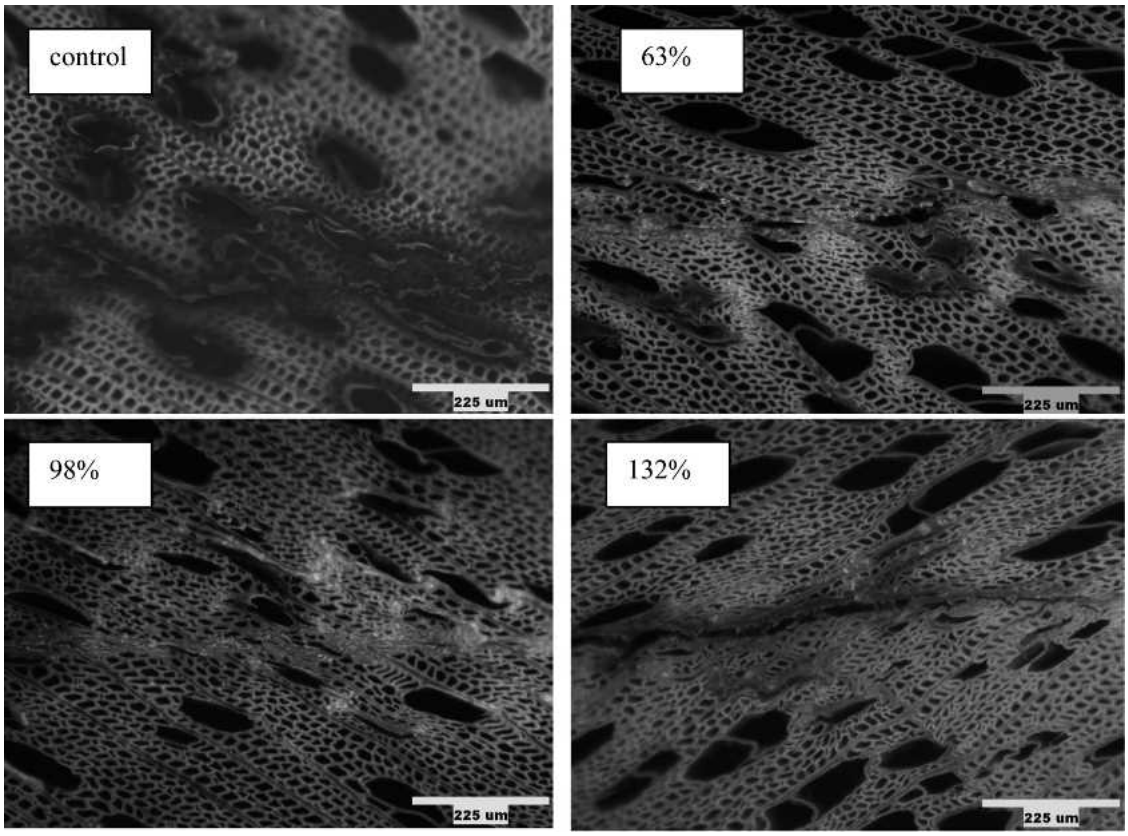

FIGURE 5. The PF adhesive penetration in the control and the VTC wood specimens of different degrees of densification.

TABLE 3. *Modulus of elasticity of the control and VTC wood specimens (standard deviations in parentheses).*

Degree of densification	E (GPa)
0% (control)	8.7 (0.59)
63%	11.2 (2.27)
98%	16.0 (2.39)
132%	19.9 (3.41)

The average G_{IIc} was the lowest for the bonded control specimens. Mode-II crack initiation toughness was the highest for the VTC wood specimens with 98% densification. The G_{IIc} may have reached a plateau in the bonded control wood of about 0.38 kN/m. For the VTC specimens, G_{IIc} continued to increase with crack length. This increase occurred because the crack propagated from the interface into the wood tissue of the VTC wood specimens, whereas in the control wood specimen, the crack initiated in the interface and propagated within the interphase. It should also be noted that as the crack propagated, the difference between G_{IIc} of the control

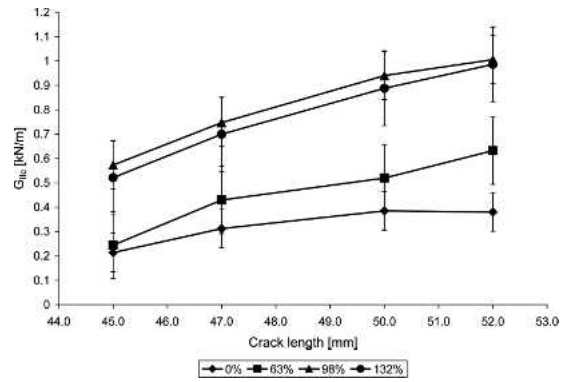

FIGURE 6. The relationship between the crack length a and the mode II interlaminar fracture toughness G_{IIc} for the ONF specimens with the different degrees of densification.

TABLE 4. *Average values of G_{IIc} for the ONF specimens at different crack lengths and p-values .*

	45 mm		47 mm		50 mm		52 mm	
Degree of densification	Average G_{II} [kN/m]	p-value	Average G_{II} [kN/m]	p-value	Average G_{II} [kN/m]	p-value	Average G_{II} [kN/m]	p-value
0% (control)	0.214	0.0511	0.312	0.0398	0.385	0.0042	0.380	0.0041
63%	0.295		0.433		0.456		0.632	
98%	0.491		0.636		0.806		1.006	
132%	0.414		0.573		0.769		0.986	

and VTC wood specimens became significantly different (Table 4) at the 95% confidence level.

End–notched Flexure

Determination of the G_{IIc} by the ENF test was influenced by crack stability problems. Since the crack propagation was accelerating and decelerating, and in some cases arresting, it was impossible to control the crack increments. Because of this unstable or stick-slip growth, different propagation points were determined for each specimen. The resulting G_{IIc} for four VTC specimens with 132% degree of densification is presented in Fig 7 as an example of problems with the ENF geometry. Two specimens reached plateaus similar in magnitude to the ONF results; two specimens did not reach a plateau. Also, in all control and VTC specimens, the crack initiated in the interface and then propagated into the wood.

Another problem within the ENF method was

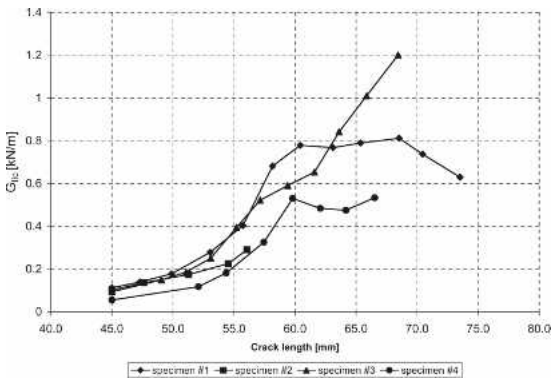

FIGURE 7. The relationship between the crack length *a* and the mode II interlaminar fracture toughness G_{IIc} for the ENF specimens with the degree of densification 132%.

that lower G_{IIc} values at crack initiation were observed, compared with the ONF method, again due to instability of the ENF geometry. Because of fast crack propagation at the beginning of crack growth, it was difficult to determine the correct point of initiation. Szekrenyes (2005) also observed a significantly lower G_{IIc} of crack initiation obtained by the ENF method in comparison with the ONF method for glass/polyester specimens.

Other researchers (Yoshihara and Ohta 2000; Yang and Sun 2000; Yoshihara 2003) have found that the initial crack length-to-span ratio of the ENF specimen controls the manner in which the delamination crack extends. Cantwell (1997) studied the effect of varying crosshead displacement rate on the value of G_{IIc} obtained by ENF specimens. The study concluded that G_{IIc} tends to increase with increasing crosshead displacement rate before reaching a plateau at high rates. The same results were obtained by Kusaka et al (2006); the mode-II interlaminar fracture toughness of the Zanchor reinforced composites increased with the increasing loading rate with ENF specimens. Therefore, we concluded that the ENF test used in the present study was not suitable for investigating crack initiation and crack propagation in laminated wood structures.

CONCLUSIONS

The results of this study established that wood densification with the VTC process did not degrade the ability of the surface of VTC samples to properly bond with PF adhesive. The mode-II adhesive fracture toughness of VTC wood was superior to that of the untreated wood. The re-

duced effective penetration of the PF adhesive into the VTC wood was not crucial for the adhesion.

The effective penetration of the PF adhesive was greatest in the case of the control wood, and for VTC wood it decreased with increasing degrees of densification. Microscopic examination of the bonded interphase showed that the location of the adhesive changed with the degree of densification as a consequence of the closed structure of the densified specimens. The adhesive followed the path of least resistance. Because of the collapsed vessels in the VTC wood specimens, the adhesive entered the lumens of fibers and rays.

The average fracture toughness was the lowest for the bonded control specimens and increased for the VTC wood specimens. For the control specimens, the crack propagated within the interphase and the toughness remained low. For the VTC specimens, the crack propagated from the interphase into the VTC wood and the toughness increased with crack length. Mode-II crack propagation in fibrous materials will follow a path close to the fiber direction, but with the lowest shear resistance (or mode-II toughness). In control specimens, that path was within the interphase. In the VTC specimens, the path was in the VTC wood, which apparently improved shear resistance compared with the control wood interphase. The fact that the crack remained in the interphase in control wood may imply that the greater adhesive penetration had depleted the interface of adhesive and limited its toughness. The toughness of control wood specimens is probably limited by the low toughness of the control wood itself. In contrast, more adhesive remained at the interface in VTC specimens. The additional adhesive probably sufficiently improved the local toughness that the crack diverted away from the interphase into the VTC wood. Despite the diversion, the toughness was higher because of the improved shear resistance of VTC wood.

Grain orientation may need to be considered, since in mode I, grain orientation significantly influences fracture toughness. Since reorientation of grain direction alters shear properties, it is likely that grain orientation will also affect mode-II crack growth along the path of lowest shear resistance. It is possible that samples with constant grain orientation would reach a plateau toughness leading to a single material parameter characterizing mode-II toughness.

The results showed that the concept of fracture mechanics can be applied to the bonded VTC wood system. The results revealed that the ONF specimen geometry can be used to discern differences in bond performance of VTC wood, however, further research is needed. The effects of surface properties, grain orientation, and specimen geometry should be studied. Moreover, the influence of testing parameters on the mode-II fracture toughness has to be investigated. While the ONF specimen geometry seems to be a promising method for mode II fracture testing of adhesively bonded wood specimens, the ENF geometry is less useful due to crack stability problems.

ACKNOWLEDGMENTS

The authors acknowledge the financial support from USDA/CSREES National Research Initiative Grant No. 2006-35504-17444 and of the Slovenian Ministry of Higher Education, Science and Technology.

REFERENCES

CANTWELL WJ (1997) The influence of loading rate on the mode II interlaminar fracture toughness of composite materials. J Compos Mater 31(14):1364–1380.

DAVIES P, BLACKMAN BRK, BRUNNER AJ (1998) Standard test methods for delamination resistance of composite materials: Current status. Adv Compos Mater 5:345–364.

EBEWELE R, RIVER B, KOUTSKY J (1979) Tapered double cantilever beam fracture tests of phenolic-wood adhesive joints, Part 1. Development of specimen geometry; effects of bondline thickness, wood anisotropy and cure time on fracture energy. Wood Fiber Sci 11(3):197–213.

FOLLRICH J, MÜLLER UM, GINDL W (2006) Effects of thermal modification on the adhesion between spruce wood (*Picea abies* Karst.) and a thermoplastic polymer. Holz Roh Werkst 64:373–376.

GAGLIANO JM, FRAZIER CE (2001) Improvements in the fracture cleavage testing of adhesively-bonded wood. Wood Fiber Sci 33(3):377–385.

GÉRARDIN P, PETRIC M, PETRISSANS M, LAMBERT J, EHRHRARDT JJ (2007) Evolution of wood surface free energy after heat treatment. Polym Degrad Stabil 92:653–657.

HUNG PC, VOLOSHIN AS (2003) In-plane strain measurement by digital image correlation. J Braz Soc Mech Sci Eng 15(3):215–221.

IMAGEJ (2007) Research Services Branch, National Institute of Mental Health, Bethesda, MD. Available on: http://rsb.info.nih.gov/ij/.

JENNINGS JD, ZINK-SHARP A, KAMKE FA, FRAZIER CE (2005) Properties of compression densified wood. Part I. bond performance. J Adhes Sci Technol 19(13-14):1249–1261.

———, ———, FRAZIER CE, KAMKE FA (2006) Properties of compression densified wood. Part II. surface Energy. J Adhes Sci Technol 20(4):335–344.

KAMKE FA (2004) A novel structural composite from low density wood. Proc. 7th Pacific Rim Bio-Based Composites Symposium, Nanjing, China, Oct. 31–Nov. 2. Pp 176–185.

———, SIZEMORE H (2005) Viscoelastic thermal compression of wood. U.S. Patent Application No. US2005/006004AI, Jan. 13, 2005

KUSAKA T, HOJO M, FUKUOKA T, ISHIBASHI M (2006) Effect of strain rate on the interlaminar fracture toughness of Zanchor reinforced composites. J Phys IV France 134: 1105–1111.

KUTNAR A, KAMKE FA, SERNEK M (2008) Density profile and morphology of viscoelastic thermal compressed (VTC). Wood Sci Technol (accepted May 2008).

NAIRN JA (2006) On the calculation of energy release rates for cracked laminates with residual stresses. Int J Fracture 139:267–293.

PETRISSANS M, GERARDIN P, ELBAKALI I, SERRAJ M (2003) Wettability of heat-treated wood. Holzforschung 57:301–307.

SCHMIDT RG (1998) Aspects of wood adhesion: applications of wood C CP/MAS NMR and fracture testing. PhD dissertation, Virginia Tech, Blacksburg, VA.

SERNEK M, KAMKE FA, GLASSER WG (2004) Comparative analysis of inactivated wood surfaces. Holzforschung 58: 22–31.

———, RESNIK J, KAMKE FA (1999) Penetration of liquid urea-formaldehyde adhesive into beech wood. Wood Fiber Sci 31(1):41–48.

SZEKRENYES A (2005) Delamination of composite specimens. PhD Dissertation. Department of Applied Mechanics, Budapest University of Technology and Economics,

———, UJ J (2005) Mode-II Fracture in E-glass–polyester composite. J. Compos Mater. 39(19):1747–1768.

WANG J, QIAO P (2003) Fracture toughness of wood–wood and wood–FRP bonded interfaces under mode-II loading. J Compos Mater 37(10):875–897.

YANG Z, SUN CT (2000) Interlaminar fracture toughness of a graphite/epoxy multidirectional composite. J Eng Mater-T ASME 122:428–433.

YOSHIHARA H, OHTA M (2000) Measurement of mode II fracture toughness of wood by the end-notched flexure test. J Wood Sci 46:273–278.

——— (2003) Resistance curve for the mode II fracture toughness of wood obtained by the end-notched flexure test under the constant loading point displacement condition. J Wood Sci 49:210–215.

———, FURUSHIMA T (2003) Shear strengths of wood measured by various short beam shear test methods. Wood Sci Technol 37:189–197.